# Compression Properties of Two-dimensional Wood-based Dowel Lattice Structure Filled with Polyurethane Foam

Gaoyuan Ye, Qingyuan Xu, Yanpeng Cheng, Zixuan Fan, Qi Li, Jiankun Qin, Shuguang Li, and Yingcheng Hu *

Foam-filled two-dimensional lattice structures were designed, and their compression performance was studied relative to corresponding structures without the foam. The experimental results showed that the compressive load of foam-filled lattice structures improved greatly compared with foam-unfilled specimens. The specific energy absorption (SEA) of foam-unfilled specimens exceeded that of the corresponding foam-filled lattice structure. The maximum energy absorption efficiency of the foam-unfilled lattice structure exceeded 1.5, while that of the foam-filled lattice structure was less than 1. The theoretically predicted compression performance was close to the experimental results. The wood-based lattice structure exhibited excellent specific strength and stiffness compared with other structures.

*Keywords: Lattice structure; Compression property; Specific strength; Specific stiffness*

*Contact information: Key Laboratory of Bio-based Material Science and Technology of the Ministry of Education of China, College of Material Science and Engineering, Northeast Forestry University, Harbin 150040, China; *Corresponding author: yingchenghu@nefu.edu.cn*

## INTRODUCTION

A lattice structure is composed of nodes and bar elements connected between nodes. It features high specific strength, high specific stiffness, good energy absorption performance, and other excellent properties. Such structures have been applied in aerospace, the automotive industry, for high-speed railways, and in other fields (Fan *et al*. 2009; Fan *et al.* 2010; Yang *et al.* 2013). Lattice structures have many configurations, such as tetrahedral (Kooistra *et al.* 2004), pyramidal (Zok *et al.* 2004; Biagi and Bart-Smith 2007; Queheillalt and Wadley 2009), and the Kagome (Zhang *et al.* 2018; Lee *et al.* 2019). Wang *et al.* (2010) fabricated a mold and used the hot-pressing technology to integrate carbon fibers into a pyramidal lattice structure for compression experiments. The failure mode of the lattice structure was mainly yield and fracture of the core. Zhang *et al.* (2012) fabricated a carbon fiber tetrahedral lattice structure with thermally expanding silicone rubber; this lattice structure has a higher specific strength than several metal lattice structures. Queheillalt and Wadley (2005) used a stainless-steel hollow tube as core to prepare a hollow lattice through welding. The hollow lattice had performance features beyond those of the solid lattice, such as an improved anti-buckling ability. Sun and Gao (2013) improved the carbon fiber pyramid lattice structure, and this improved structure achieved better comprehensive performance. Fan et al. (2014) prepared a pyramidal lattice structure with glass fiber and conducted a compression experiment, demonstrating that the multi-level lattice structure had a higher ductility and energy absorption efficiency with regard to energy absorption.

Lattice structures generally consist of metal or carbon fibers, and research on wood-based lattice structures is relatively rare. In this experiment, wood was used to investigate the compression performance of lattice structures with cores of different length. The structure of the lattice filled with polyurethane foam was investigated *via* compression tests. The specific strength, specific stiffness, and other characteristics of the lattice structures were analyzed.

## EXPERIMENTAL

### Preparation of Two-Dimensional Lattice Structure

Oriented strand board (OSB) was used as the panel for the lattice structure. It was purchased from Dongfang Port International Wood, Ltd. (Beijing) and made from pine-wood shavings. Birch dowel (Harbin Tengzhan Wood Industry, Ltd., Harbin, China) was used as the core. The OSB was drilled, and the core was inserted and glued with epoxy resin. The preparation process is shown in Fig. 1. After the two-dimensional lattice structure was prepared, materials A and B (consisting of polyurethane foam) were mixed, stirred for 15 s, and poured into the core layer of the lattice structure to obtain the corresponding foam-filled lattice structure. A foam density of 20kg/m$^3$ was used. The E-44 type epoxy resin was purchased from Nantong Xingxing Synthetic Materials, Ltd., Harbin, China. Foam was purchased from Shandong Yisheng Polyurethane Foam, Ltd., Harbin, China.

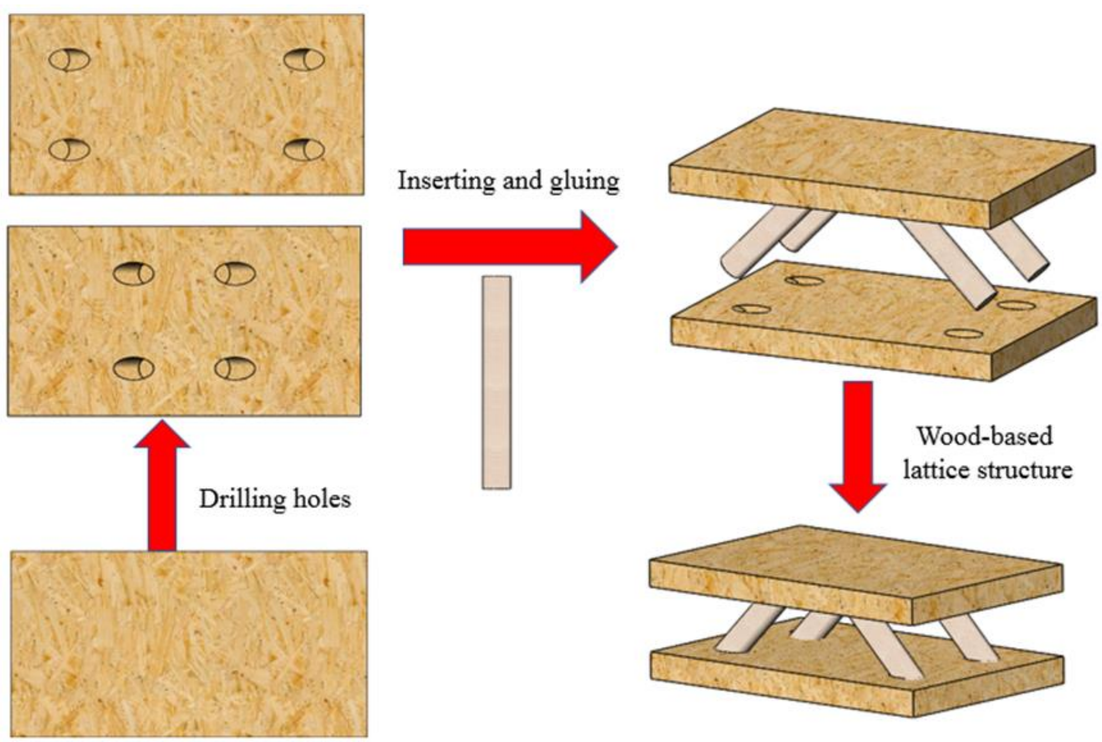


**Fig. 1.** Preparation process of the lattice structure

## Experiment

Three sizes of lattice structures and their corresponding foam-filled specimens were compressed. The sizes of the specimens are shown in Table 1. The A, B, and C lattice structures filled with foam were named A1, B1, and C1 lattice structures, respectively. The length and width of the A, B, and C specimen panels were 150 × 50 mm, 220 × 50 mm, and 300 × 50 mm, respectively. A schematic diagram of the lattice structure is shown in Fig. 2. *L* is the length of the core, *d* is the diameter of the core, *ω* is the included angle between the core and the panel, and *t* is the spacing between the core.

**Table 1.** Size and Relative Density of the Lattice Structure

| Type | *t* (mm) | *ω* | *d* (mm) | *l* (mm) | Theoretical $\bar{\rho}$ | Actual $\bar{\rho}$ | Diameter to length ratio |
|---|---|---|---|---|---|---|---|
| A | 20 | 45 | 6 | 42 | 1.61% | 1.06% | 0.14 |
| B | 20 | 45 | 6 | 102 | 0.87% | 0.73% | 0.06 |
| C | 20 | 45 | 6 | 162 | 0.59% | 0.53% | 0.04 |

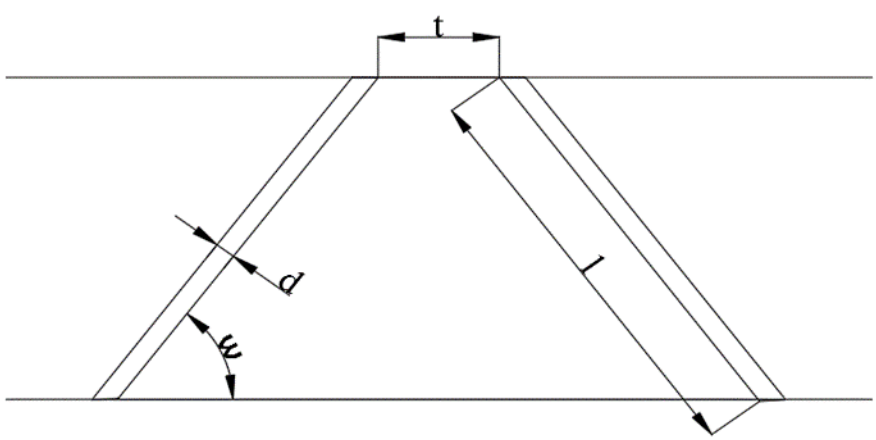


**Fig. 2.** Schematic diagram of the lattice structure

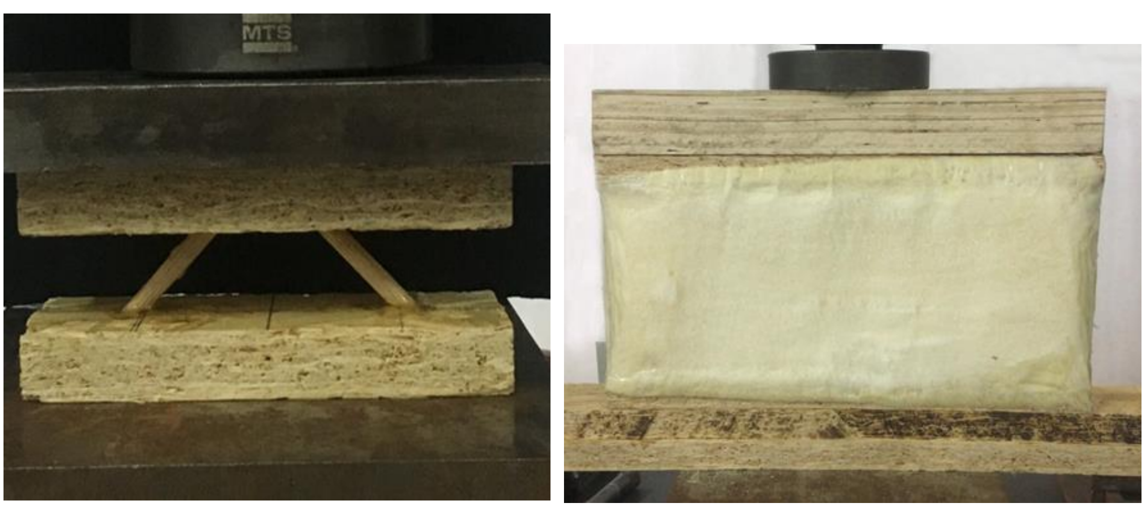


**(a)** **(b)**

**Fig. 3.** Compression diagram of lattice structure of (a) unfilled and (b) filled foam

Four test pieces were used for each group of A, B, C, A1, B1, and C1 lattice structures. The quasi-static compression response of samples was studied. Figure 3 shows the compression test diagram, indicating that the compression force was applied from the top of the structure. The compression experiment was conducted on a universal mechanical testing machine (Shenzhen Sans Material Testing Co., Ltd, Microcomputer controlled electronic universal testing machine C61.104, Shenzhen, China) according to ASTM C365/C365M-11a (Cote *et al.* 2007) standard with a compression speed of 2 mm/min.

## RESULTS AND DISCUSSION

### Compression Experimental Results

The load-displacement curves of the three lattice structures A, B, and C and the corresponding foam-filled lattice structures A1, B1, and C1 are shown in Fig. 4. Part (a) shows two load-displacement curves: the load-displacement curve of the A lattice represents one type, and those of B and C represent a different type. The load-displacement curve of the A lattice has three stages: an elastic stage, a platform stage where the load gradually decreased, and a densification stage. When the load was first applied, the force increased rapidly with displacement. After the force reached the maximum strength, the core was destroyed, and the force decreased with displacement, finally entering the densification stage. The load-displacement curves of B and C lattice have two stages: an elastic stage and a stage when the load suddenly decreases with displacement. When entering the elastic stage, the force increased rapidly with displacement. After the force reached the peak force, the core broke and the load decreased suddenly. The reason for these two load-displacement curves is as follows: the core diameter to length ratio of the A lattice is large. When the load reached a maximum, the core was damaged but did not break suddenly. The core diameter to length ratio of B and C lattice was small, and when the maximum load had been reached, the core broke, resulting in the failure of the bearing capacity. Figure 4 shows that the peak load followed the order A > B > C. The reason is that the greater the diameter to length ratio of the core, the greater the peak load will be, and the diameter to length follows A > B > C; therefore, the peak load follows A > B > C.

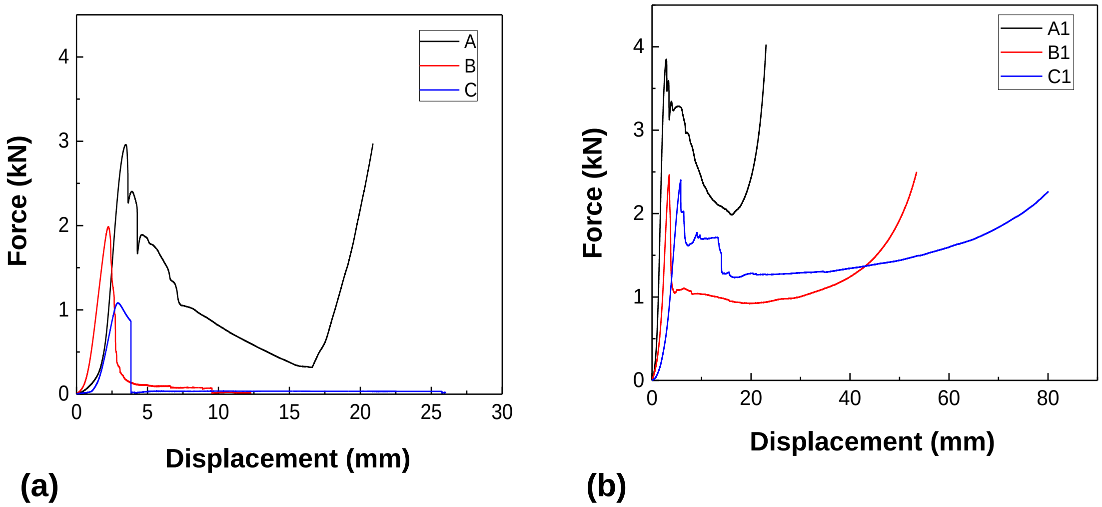


**Fig. 4.** Load-displacement curves of lattice structure of (a) unfilled and (b) filled foam (the core lengths of A, B, and C structures are 42mm, 102mm, and 162mm, respectively, while the structures of A1, B1, and C1 are obtained by filling the foam with A, B, and C structures, respectively)

The failure diagrams of lattice structures of A, B, and C are shown in Fig. 5. The core of lattice A suffered shear failure in the middle and upper part; the core of lattice B suffered bending failure in the middle part; the core of lattice C suffered buckling failure in the middle part, which resulted in core fracture. The failure modes of the lattice structure were consistent with the corresponding load-displacement curves.

**(a)** Lattice structure

**(b)** Destructive A lattice structure

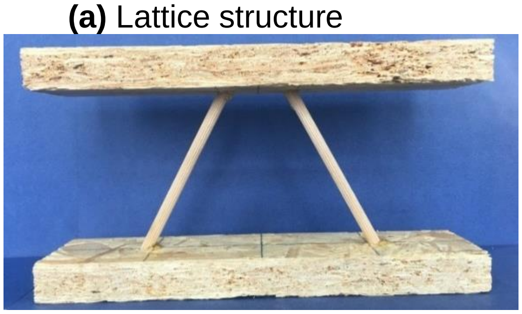

**(c)** B lattice structure

**(d)** Destructive B lattice structure

**(e)** C lattice structure

**(f)** Destructive D lattice structure

**Fig. 5.** The damage map of lattice structure of unfilled foam

The load-displacement curves of A1, B1, and C1 lattice are shown in Fig. 4b. The three curves in Fig. 4b all have three stages: an elastic stage, a plateau stage, and a densification stage. The difference is that the A1 lattice height decreased slowly when the load reached the minimum value after the peak load, while B1 and C1 immediately decreased to the minimum value, which is identical to the corresponding lattice without filling foam. The peak force of A1 was largest, and those of B1 and C1 were close. The reason for this is that the core length to diameter ratio of the A1 lattice structure was the largest, and the foam effect was enhanced; therefore, the peak force was the largest; the diameter to length ratios of B1 and C1 lattice were not very different, and if there was no foam enhancement effect, the foam filled C1 lattice would buckle due to the small length to diameter ratio, leading to a lower peak force than that of B1 lattice without foam filling. However, due to the foam filling, the C1 core was restrained from buckling, and a specific enhancement effect was achieved; therefore, the peak forces of both the C1 and B1 lattices were close to each other.

Figure 4b shows that the sequence of entering the densification stage follows A1, B1, and C1. Due to the poor filling foam performance, a specific distance needs to be compressed to enter the densification stage. Therefore, the higher the lattice structure, the longer the compression distance when entering the densification stage. Figure 6 shows the failure diagram of the foam-filled lattice, which indicates that the core of the A1 lattice was damaged in the foam without penetrating the foam, while the cores of both the B1 and C1 lattice were fractured and pierced the outer surface of the foam.

**(a)** A1 lattice structure

**(b)** Destructive A1 lattice structure

**(c)** B1 lattice structure

**(d)** Destructive B1 lattice structure

**(e)** C1 lattice structure

**(f)** Destructive C1 lattice structure

**Fig. 6.** Damage map of lattice structure of filled foam

The force-displacement curves of foam-filled specimens, the corresponding unfilled foam lattice structure specimens, and the corresponding force displacement curves of the foam are shown in Fig. 7. The figure shows that the elastic modulus of the lattice structure with foam filling and that of the unfilled lattice structure in the elastic phase were largely identical, since the core was subject to stress during the elastic phase. For the lattice structures of A1 and B1, foam played a strengthening role during the elastic stage; therefore, the peak load of the lattice structures of A1 and B1 exceeded that of A and B lattice structures. With regard to the C1 lattice structure, foam played an inhibitory role in the core buckling and enhanced the core layer during the elastic stage; therefore, the peak force of the C1 lattice far exceeded that of C lattice. When entering the second stage, B1 and C1 lattice structures entered the platform stage. At this stage, foam played a major role, because the load-displacement curves of B1 and C1 lattices and that of the corresponding foam basically coincided. With regard to the A1 lattice structure, the foam and core augment each other during the platform phase. Finally, all foam-filled lattice structures entered the densification stage. The enhancement effect of the foam on the lattice structure was studied from the peak force direction. Table 2 shows the peak force of the lattice structure, indicating that the peak force of the C lattice structure increased most (by 145%), followed by the peak force of the A and B lattices, which increased by 45% and 42%, respectively.

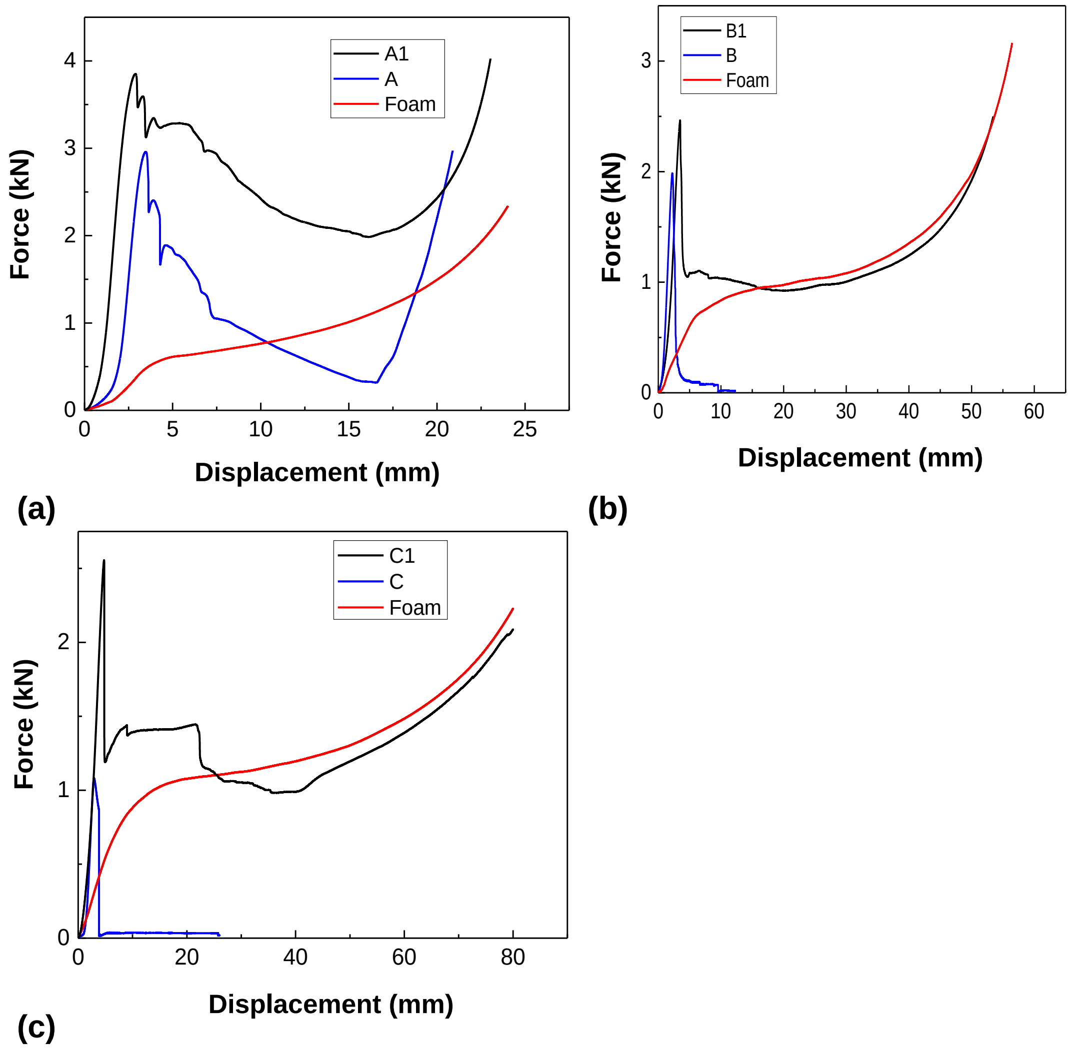


**Fig. 7.** Load-displacement curve of lattice structure and corresponding foam for A and A1 (b) B and B1, and (c) C and C1(A1, B1 and C1 lattice structures are foam filled structures, while A, B and C structures are not filled with foam)

To investigate the reinforcing effect of the foam on the lattice structure, the load-displacement figure of the filled foam lattice structure and the unfilled foam lattice structure, as well as the load-displacement curve of the foam are shown in Fig. 8. The compression performance of the A1 lattice structure was not the sum of the compression performance of the A lattice structure and the foam; however, it exceeded the sum of the compression performance of both. The compression performance of the B1 and C1 lattice structures was approximately the same as the sum of the corresponding foam and both B and C lattice compression performance. The reason why A1 appeared to be enhanced is that the performance of the foam was poor, and the core diameter ratio of the A lattice structure was large. When the A lattice structure was in the elastic phase, the reinforcing effect of the foam on the core did not differ strongly from that of the core and the foam. However, during the platform stage, the core broke but did not fracture, and the foam enhanced the core. The reason for this situation in the B1 and C1 lattice structures is that during the elastic phase, the reinforcing effect of the foam on the core in the B1 lattice structure does not differ strongly from the sum of the core and foam properties. During the platform stage, the core of the B1 lattice structure fractures and the foam was active alone. During the elastic phase, the load of the foam on the C1 lattice structure increased greatly; however, the displacement during the elastic phase was small. During the platform stage, the core of C1 lattice structure fractured, and only the foam was active; therefore, there is no case of 1 + 1>2. Note that in the foam-filled test piece, not all filled test pieces will achieve the 1 + 1>2 effect.

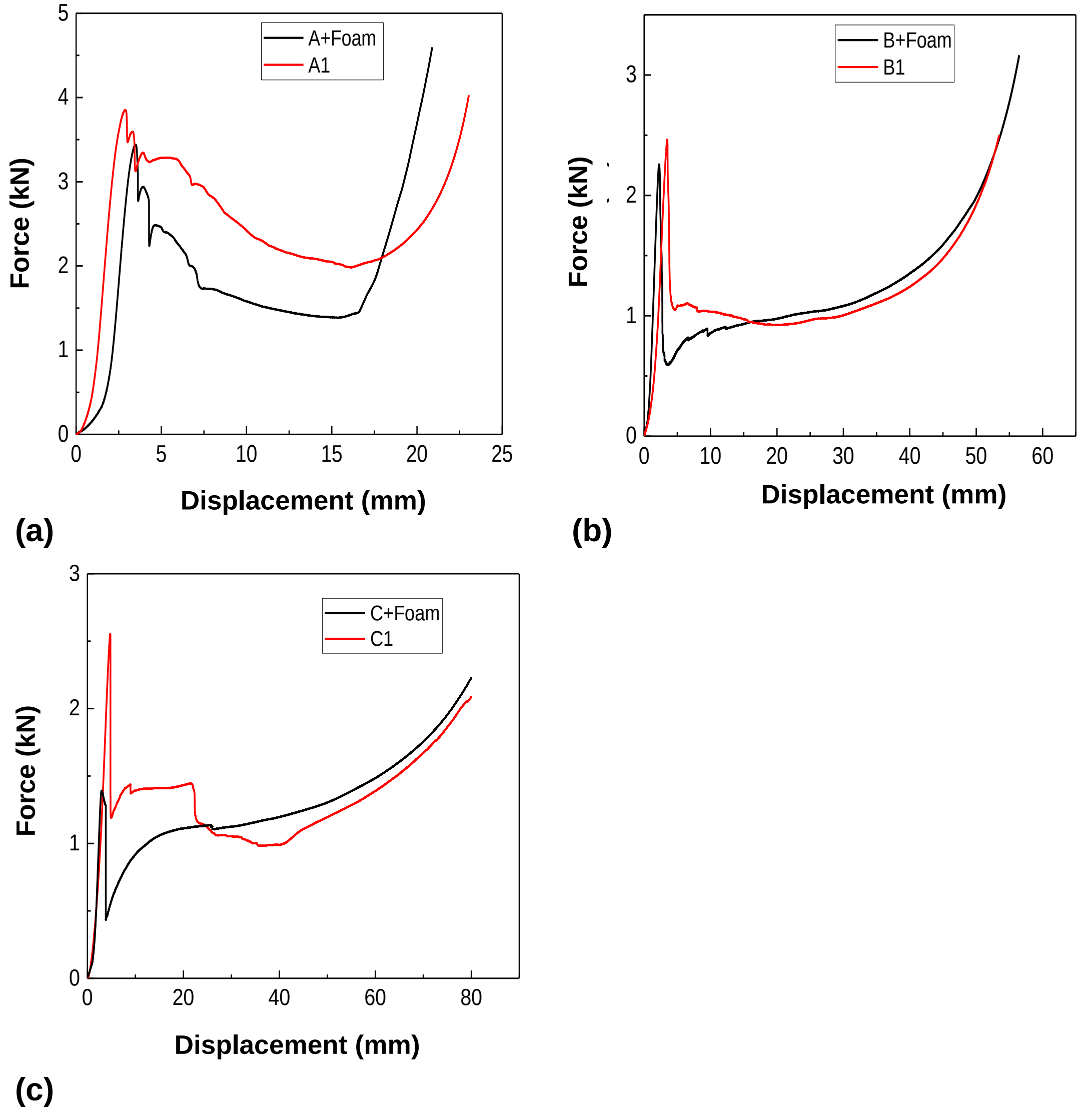


**Fig. 8.** Load-displacement curve of lattice structure for A+foam and A1 (b) B+foam and B1, and (c) C+foam and C1

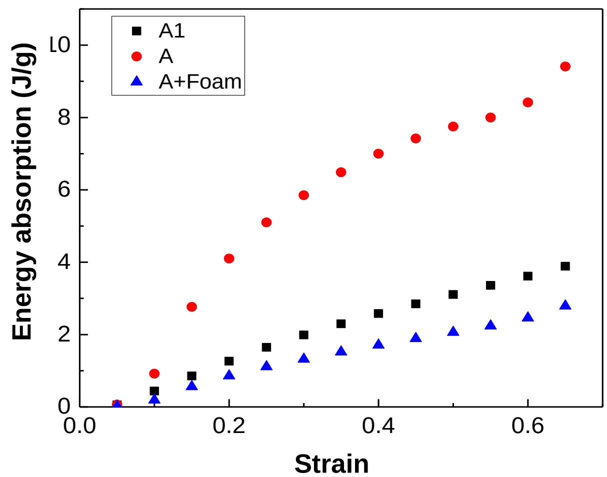


**Fig. 9.** Specific energy absorption of the lattice structure

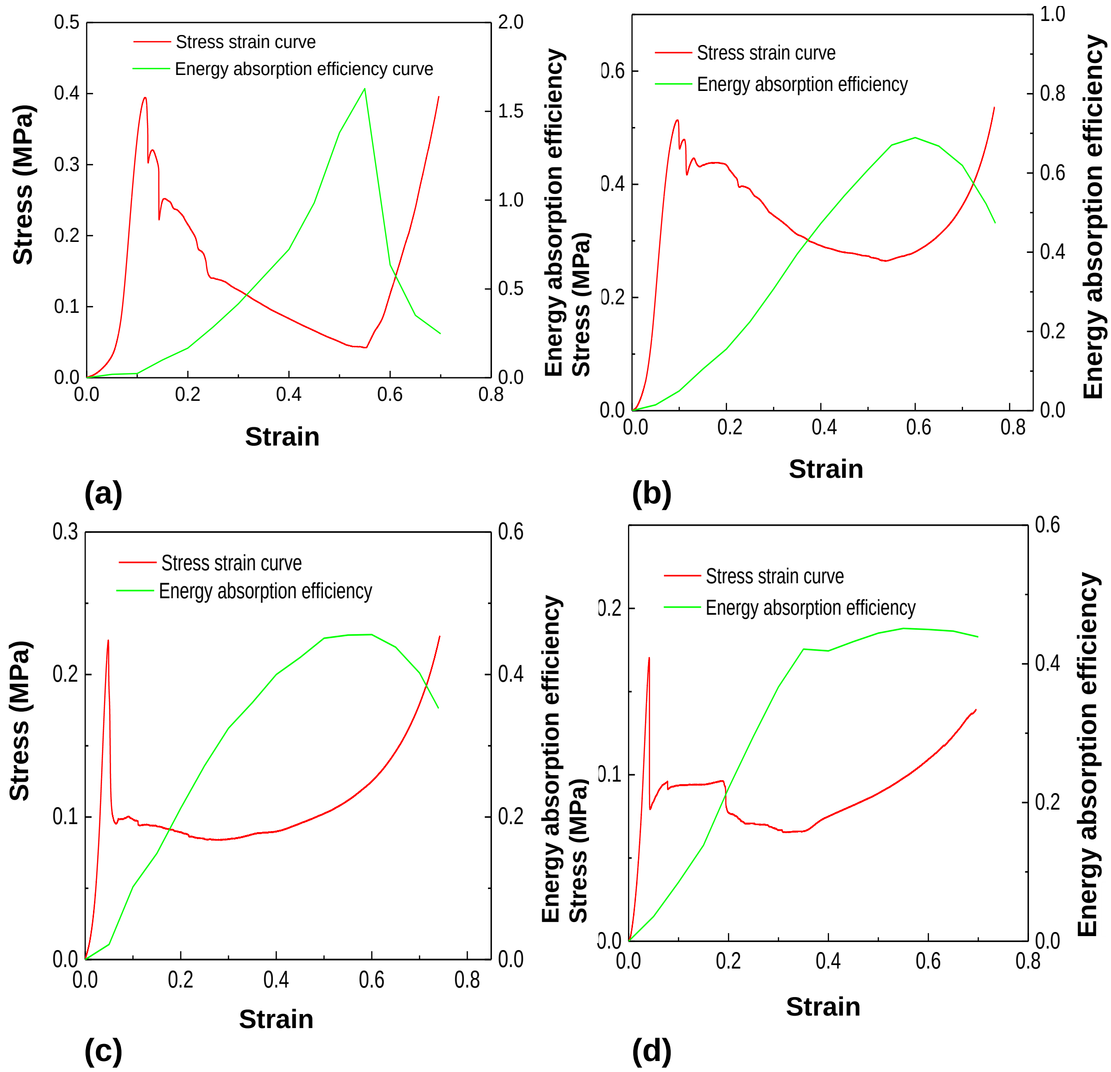


**Fig. 10.** Energy absorption efficiency and stress strain curve of lattice structure for(a) A, (b) A1, (c) B1, and (d) C1

**Table 2.** Peak Force of Lattice Structure

| Type | Peak Force of Unfilled Foam Structures (N) | Peak Force of Filled Foam Structures (N) | Percentage of Enhancement |
|---|---|---|---|
| A | 2740 | 3970 | 45% |
| B | 1893 | 2686 | 42% |
| C | 1108 | 2715 | 145% |

Filling of the structure with foam increased the energy absorption performance of the test piece, and also increased its quality. The specific energy absorption (SEA) of the sandwich structure is related to the quality of the core layer; therefore, it is more practical to compare the SEA of the sandwich structure. The SEA is defined as the energy absorption capacity per unit mass of the core layer. Since both B and C specimens have no densification stage, only type A specimens were analyzed. Figure 9 shows the SEA of the A lattice structure, the A1 lattice structure, and the SEA sum of the foam and the A lattice structure. The SEA of the A lattice structure exceeded that of A1, and the SEA sum of the A lattice structure and the foam was smallest. The main reason is that the mass increase effect of the foam exceeded the load increase effect it caused. Therefore, for the SEA, it is not necessary that the foam-filled test piece is larger than the unfilled test piece.

The energy absorption efficiency refers to the ratio of the absorbed energy to the stress of the lattice structure (Simon *et al.* 2016); it was calculated as follows,

$$E = \frac{\int_{\varepsilon_1}^{\varepsilon_2} \sigma(\varepsilon)d\varepsilon}{\sigma(\varepsilon)} \tag{1}$$

where $E$ is the energy absorption efficiency, and $\sigma$ is the strength of lattice structure. The strain corresponding to the maximum value of the energy absorption efficiency is the strain of the densification point. The energy absorption efficiency of the lattice structure is shown in Fig. 10. With increasing strain, the energy absorption efficiency doesn't simply increase. Rather, it only increases initially, followed by a decrease. As shown in Fig. 10, during the elastic phase and the platform phase, the energy absorption efficiency increased rapidly and reached a maximum near the densification point. After entering the densification phase, the stress increased rapidly, and its rate of increase exceeded the corresponding energy absorption; therefore, the energy absorption efficiency decreased. The maximum energy efficiency of the A lattice was approximately 1.5, that of the A1 lattice was approximately 0.7, and that of the B1 and C1 lattices was approximately 0.5. The reason why the energy absorption efficiency of the A lattice exceeded 1.5 is that in the platform stage, the stress continued to decrease, and the energy absorption increased. When the densification point had been reached, the stress was minimized, and the energy absorption far exceeded the stress value at this point. Therefore, the energy absorption efficiency of the A lattice was higher than 1.5.

## Prediction and Analysis of the Lattice Structure Compression Performance

The lattice structure can be simplified to a mechanical model. A single cell has two cores, and two cores experience the same force; therefore, the force of a single core was analyzed, as shown in Fig. 11. When the core is crushed (Wang *et al.* 2017),

$$F_a = \frac{1}{4}\pi d^2 E_m \frac{\delta sin\omega}{l} \tag{2}$$

$$F_s = \frac{12E_m I\delta\cos\omega}{l^3} \quad (3)$$

$$F = F_a sin\omega + F_s cos\omega = \frac{\pi d^2 E_m \delta}{4l}\left[sin^2\omega + \frac{3}{4}\left(\frac{d}{l}\right)^2 cos^2\omega\right] \quad (4)$$

where $E_m$ represents the elastic modulus of the core material; $\delta$ is the displacement of z direction; *I* is the inertia moment of the cross section; *l* is the core length; and *d* is the core diameter.

The diameter to length ratio was small; therefore, the influence of the shear force was ignored, and the resultant force is:

$$F = \frac{\pi d^2 E_m \delta}{4l} sin^2\omega \quad (5)$$

The strength of the lattice structure can be expressed as:

$$\sigma = \frac{2F}{S} = \frac{\pi d^2 E_m \delta}{4bl(lcos\omega + t)} sin^2\omega \quad (6)$$

The strength of the core can be expressed as:

$$\sigma_1 = E_m \varepsilon = E_m \frac{\delta\sin\omega}{l} \quad (7)$$

The relative density of the lattice structure can be expressed as:

$$\bar{\rho} = \frac{\pi d^2}{4b(lcos\omega + t)sin\omega} \quad (8)$$

The relative density and the strength of the core are introduced into the strength formula of lattice structure, which yields:

$$\sigma = \sigma_1 \bar{\rho} \sin^2\omega \quad (9)$$

When the core is subject to buckling failure, the axial force of the core is:

$$F_a = \frac{4\pi^2 E_m I}{l^2} \quad (10)$$

Ignoring the tangential force on the core, the external force of the lattice structure is:

$$F = \frac{8\pi^2 E_m I}{l^2} sin\omega \quad (11)$$

The strength of the structure can be expressed as:

$$\sigma = \frac{F}{S} = \frac{\pi^3 d^4 E_m}{16bl^2(lcos\omega + t)} sin\omega \quad (12)$$

Eq. (8) is substituted into Eq. (12):

$$\sigma = \frac{\pi^2 d^2 E_m}{4l^2} sin^2\omega \quad (13)$$

The formula for defining the elastic modulus is:

$$E = \frac{\sigma}{\varepsilon} \tag{14}$$

The strain of lattice structure is:

$$\varepsilon = \frac{\delta}{l\sin\omega} \tag{15}$$

Substituting Eq. (6), (8), and (15) into Eq. (14) yields the equivalent elastic modulus of the lattice structure:

$$E = E_m\bar{\rho}sin^4\omega \tag{16}$$

Table 3 shows the theoretical compression performance and actual compression performance of different lattice structures. The core strengths of lattice structure A, B, and C were 52.49 MPa, 44.39 MPa, and 19.19 MPa; the core elastic modulus of lattice structure A, B, and C was 3753 MPa. The A lattice structure had the highest strength; the elastic modulus of the B lattice was largest; the C lattice structure had the lowest strength and elastic modulus.

The maximum errors of the lattice structure strength and elastic modulus were 28.6 and 24.1% respectively, both of which are within acceptable limits. The reason for the difference between the theoretical performance and the actual performance is that the wood is orthotropic, and the properties cannot guarantee the same performances. Experimental errors during the experimental process will also impact the experimental results.

**Table 3.** Theoretical Compression Performance and Actual Compression Performance of Lattice Structure

| Type | Relative Density | Theoretical Strength (MPa) | Actual Strength (MPa) | Error | Theoretical Elastic Modulus (MPa) | Actual Elastic Modulus (MPa) | Error |
|---|---|---|---|---|---|---|---|
| A | 1.06% | 0.28 | 0.39 | -28.2% | 9.95 | 8.02 | 24.1% |
| B | 0.73% | 0.16 | 0.18 | -11.1% | 6.85 | 8.74 | -21.6% |
| C | 0.53% | 0.05 | 0.07 | -28.6% | 5.54 | 6.11 | -9.3% |

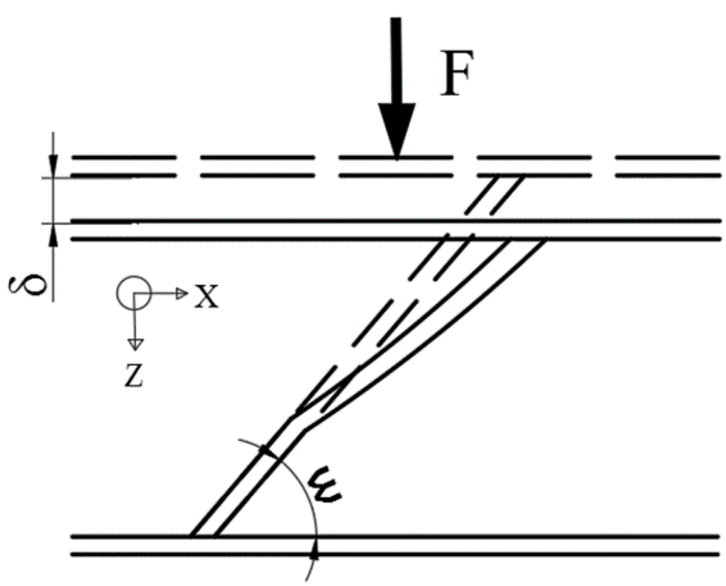


**Fig. 11.** Force analysis of lattice structure

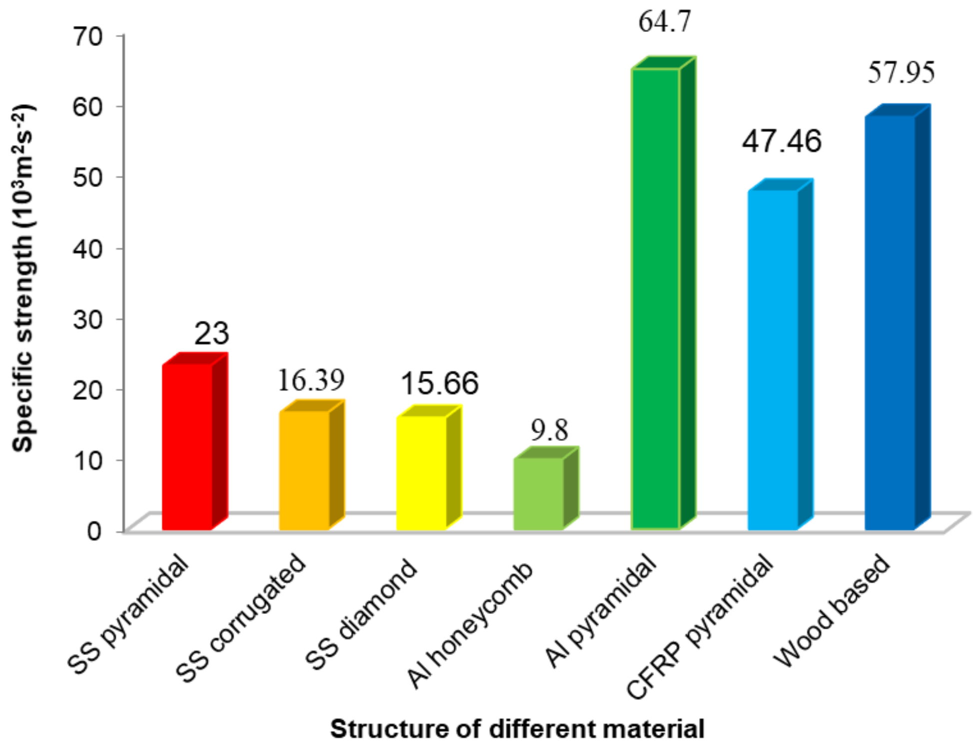


**Fig. 12.** Specific strength of different structure

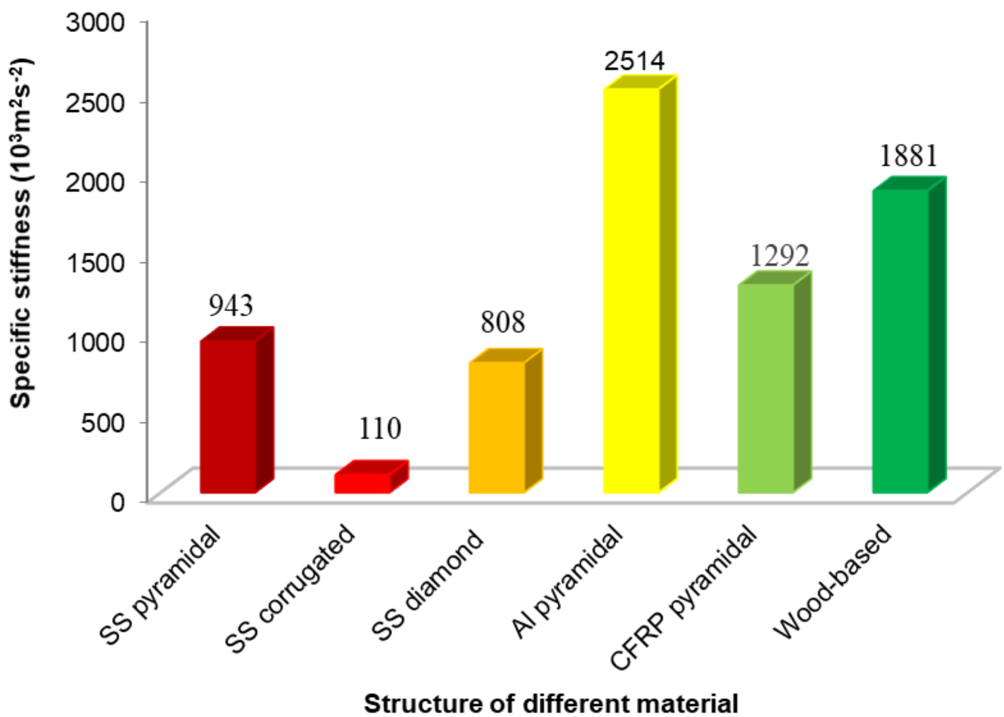


**Fig. 13.** Specific stiffness of different structure

## Comparison of Specific Strength and Stiffness

A shorter and thicker core can withstand a higher strength. Considering the core layer quality and core layer volume, it is more practical to use the specific strength and specific stiffness to represent the compression performance of the lattice structure. Both the specific strength and specific stiffness of the three test pieces are shown in Table 4. The A lattice structure had the largest specific strength. Although its core layer density was large, its ultimate strength was also relatively large; therefore, its specific strength was also large, followed by the B lattice structure, and finally the C lattice structure. The B lattice structure had the largest specific stiffness, followed by C, and then A. The specific strength of the wood-based lattice and other structures is shown in Fig. 12. The aluminum pyramidal lattice (Queheillalt *et al.* 2008) was strongest in all listed structures, but the wood-based lattice could compete with its strength. The wood-based lattice was even stronger than the specific strength of the carbon fiber reinforced plastic (CFRP) lattice structure (Wang *et al*. 2010) and aluminum honeycomb (Yan *et al*. 2015). This fully demonstrates the superiority of the wood-based lattice with regard to its specific strength. Figure 13 shows a graph of the specific stiffness of the wood-based lattice and other material structures. The specific stiffness of the wood-based lattice is second only to that of the aluminum pyramidal lattice, and higher than the CFRP lattice and a stainless-steel structure (Cote *et al.* 2006, 2007). The wood-based lattice has advantages with regard to specific stiffness and specific strength compared with other structures and materials.

**Table 4.** Specific Strength and Stiffness of the Lattice Structure

| Type | Specific Strength ($10^3 m^2 s^{-2}$) | Specific Stiffness ($10^3 m^2 s^{-2}$) |
|---|---|---|
| A | 57.95 | 1191.68 |
| B | 28.79 | 1881.47 |
| C | 20.77 | 1810.09 |

## CONCLUSIONS

1. Filling foam can greatly improve the load capacity of a lattice structure since the foam can support the core layer and restrain the core from buckling.
2. The specific energy absorption of foam-filled lattice structures is smaller than that of a foam-unfilled lattice structure. The reason is that the increasing effect in the foam mass exceeds the strength increasing effect it causes. The maximum energy absorption efficiency of the foam-unfilled specimen is much higher than that of the foam-filled specimen.
3. The theoretically predicted compression performance of the lattice structure is close to the actual result, with the strength error within 29% and the elastic modulus within 25%, which remains within an acceptable range.
4. The wood-based lattice structure has good specific strength and stiffness. Its specific strength and stiffness are comparable with those of an aluminum lattice structure.

## ACKNOWLEDGEMENTS

This project was supported by the Fundamental Research Funds for the Central universities (2572016EBJ1), the National Natural Science Foundation of China (31470581).

## REFERENCES CITED

ASTM C365/C365M-11a (2011). "Standard test method for flatwise compressive properties of sandwich cores," ASTM International, West Conshohocken, USA.

Biagi, R., and Bart-Smith, H. (2007). "Imperfection sensitivity of pyramidal core sandwich structures," *I. J. Sol. Struc*. 44(14), 4690-4706. DOI: 10.1016/j.ijsolstr.2006.11.049

Cote, F., Deshpande, V. S., Fleck, N. A., and Evans, A. G. (2006). "The compressive and shear responses of corrugated and diamond lattice materials," *Int. J. Sol. Struc*. 43, 6220. DOI: 10.1016/j.ijsolstr.2005.07.045

Cote, F., Fleck, N., and Deshpand, V. (2007). "Fatigue performance of sandwich beams with a pyramidal core," *I. J. Fatigue* 29, 1402. DOI: 10.1016/j.ijfatigue.2006.11.013

Fan, H., Qu, Z., Xia, Z., and Sun, F. (2014). "Designing and compression behaviors of ductile hierarchical pyramidal lattice composites," *Materials & Design*. 58, 363-367. DOI: 10.1016/j.matdes.2014.01.011

Fan, H., Fang, D., Chen, L., Dai, Z., and Yang, W. (2009). "Manufacturing and testing of a CFRC sandwich cylinder with Kagome cores," *Compo. Sci. Tech.* 69(15-16), 2695-2700. DOI: 10.1016/j.compscitech.2009.08.012

Fan, H., Zeng, T., Fang, D., and Yang W. (2010). "Mechanics of advanced fiber reinforced lattice composites," *Acta Mecha. Sini*. 26(6), 825-835. DOI: 10.1007/s10409-010-0390-z

Kooistra, G. W., Deshpande, V. S., and Wadley, H. N. G. (2004). "Compressive behavior of age hardenable tetrahedral lattice truss structures made from aluminium," *Acta Mater*. 52(14), 4229-4237. DOI: 10.1016/j.actamat.2004.05.039

Lee, S., Lee, K., Hwang, J., Cho, Y., Lee, K., Jeong, H., Park, S., Park, Y., Cho, Y., and Lee, B. (2019). "Evaluation of mechanical strength and bone regeneration ability of 3D printed kagome-structure scaffold using rabbit calvarial defect model," *Mater Sci Engi*. 98, 949. DOI: 10.1016/j.msec.2019.01.050

Queheillalt, D. T., and Wadley, H. N. G. (2005). "Cellular metal lattices with hollow trusses," *Acta Mater*. 53,303-13. DOI: 10.1016/j.actamat.2004.09.024

Queheillalt, D. T., and Wadley, H. N. G. (2009). "Titanium alloy lattice truss structures," *Mater Design* 30(6), 1966-1975. DOI: 10.1016/j.matdes.2008.09.015

Queheillalt, D. T., Murty, Y., and Wadley, H. N. G. (2008). "Mechanical properties of an extruded pyramidal lattice truss sandwich structure," *Scrip. Mater.* 58, 76.

Simon, R. G., Bates, I., Farrow, R., and Trask, R. S. (2016). "3D printed polyurethane honeycombs for repeated tailored energy absorption," *Mater Design.* 112, 172-83. DOI: 10.1016/j.matdes.2016.08.062

Sun, Y., and Gao, L. (2013). "Mechanical behavior of all-composite pyramidal truss cores sandwich panels," *Mech Mater*. 65, 56-65. DOI: 10.1016/j.mechmat.2013.06.003

Wang, B., Wu, L., Ma, L., Sun, Y., and Du, S. (2010). "Mechanical behavior of the sandwich structures with carbon fiber-reinforced pyramidal lattice truss core," *Mater. Design* 31, 2659-2663. DOI: 10.1016/j.matdes.2009.11.06

Wang, B., Hu, J. Q., Li, Y. Q., Yao, Y. T., Wang, S. X., and Ma, L. (2017). "Mechanical properties and failure behavior of the sandwich structures with carbon fiber-reinforced x-type lattice truss core," *Composite Structures* 185, 619-633. DOI: 10.1016/j.compstruct.2017.11.066

Yan, C., Hao, L., Hussein, A., Young, P., Huang, J., and Zhu, W. (2015). "Microstructure and mechanical properties of aluminium alloy cellular lattice structures manufactured by direct metal laser sintering," *Mater. Sci. Eng.* 628, 238. DOI: 10.1016/j.msea.2015.01.063

Yang, L., Fan, H., Liu, J., Ma, Y., and Zheng, Q. (2013). "Hybrid lattice-core sandwich composites designed for microwave absorption," *Mater. Design* 50, 863-871.DOI: 10.1016/j.matdes.2013.03.032

Zhang, G., Ma, L., Wang, B., Wu, L. (2012). "Mechanical behaviour of CFRP sandwich structures with tetrahedral lattice truss cores," *Compos Part B*. 43,471-6. DOI: 10.1016/j.compositesb.2011.11.017

Zhang, L., Feih, S., Daynes, S., Wang, Y., Wang, Y., Wei, J., Lu, W. (2018). "Buckling optimization of Kagome lattice cores with free-form trusses," *Mater Design*, 2018. DOI: 10.1016/j.matdes.2018.02.026

Zok, F. W., Waltner, S. A., Wei, Z., Rathbun, H. J., McMeeking, R. M., and Evans, A. G. (2004). "A protocol for characterizing the structural performance of metallic sandwich panels: Application to pyramidal truss cores," *I. J. Sol. Struc*. 41(22), 6249-6271. DOI: 10.1016/j.ijsolstr.2004.05.045

Article submitted: June 4, 2019; Peer review complete: September 2, 2019; Revised version received: September 16, 2019; Accepted: September 19, 2019; Published: September 23, 2019.
DOI: 10.15376/biores.14.4.8849-8865